Confinement Behavior of Rectangular Reinforced Concrete Prisms Simulating Wall Boundary Elements

Travis S. Welt, Ph.D., P.E.[1]; Leonardo M. Massone, Ph.D.[2]; James M. LaFave, Ph.D., P.E., M.ASCE[3]; Dawn E. Lehman, Ph.D.[4]; Steven L. McCabe, Ph.D., P.E.[5]; and Pablo Polanco[6]

Abstract: Observations following recent earthquakes, and from structural testing, indicate numerous brittle compression failures in reinforced concrete seismic-resisting walls. This is unexpected, as most seismic-resisting walls are designed to be tension-controlled. The problematic compressive response led to two independent studies, each individually aimed at identifying design and loading parameters that affect the seismic deformability of the compression regions (or boundary elements) of seismic-resisting walls. These experimental studies are combined here for a more complete understanding. Both studies used axially loaded, rectangular reinforced concrete specimens that simulate seismic-resisting wall boundary elements. The rectangular prisms were tested under cyclic axial loading or monotonic compression, with a focus on the following parameters: boundary element detailing classification, detailing of transverse reinforcement, maximum tensile strain preceding compressive demand, and cross-sectional aspect ratio. Test results indicate that expected strength and deformation capacity can be overestimated unless a rectangular hoop restrains every longitudinal reinforcing bar; use of crossties does not guarantee stability of the longitudinal reinforcement. Tensile strains of 2 and 5%, imposed prior to reaching the compressive capacity, resulted in compression strength reductions of 20 and 50%, respectively, indicating that load-history can also be important. **DOI: 10.1061/(ASCE)ST.1943-541X.0001682.**

Author keywords: Reinforced concrete; Structural walls; Earthquake engineering; Boundary elements; Boundary element detailing; Cyclic loading; Laboratory testing; Concrete and masonry structures.

Introduction

Observations from the recent Maule region earthquake in Chile have indicated surprisingly brittle failures in the compression zones (or boundary elements) of reinforced concrete (RC) seismic-resisting walls that were otherwise designed to be tension-controlled. Reconnaissance reports from Chile (EERI 2010) and subsequent related publications (Telleen et al. 2012; Wallace 2012) have noted damage in walls indicative of the occurrence of either longitudinal bar or sectional out-of-plane buckling, without any evidence of tensile yielding (e.g., uniformly spaced residual cracks). Telleen et al. (2012) have postulated that these failures are the result of a combination of factors related to boundary element confinement detailing, loading history, and building configuration. Collapse failures were fairly rare (fewer than five) during the Chile earthquake, though, and Telleen et al. (2012) have hypothesized that this may be due to ample structural redundancy in Chilean walled buildings arising from their architectural style.

Certain aspects of design and construction practice for seismic-resisting walls in Chile are similar to those from the U.S. (Telleen et al. 2012), which indicates that structures in the U.S. may be prone to similar failures. However, characteristic building architecture in Chile and the U.S. are noticeably different. Chilean walls are typically smaller in size and larger in number, distributed throughout each floor, and organized in a fishbone-type layout, whereas seismic-resisting walls in the U.S. are typically larger in size and concentrated in a central core. Although U.S. practice leads to thicker walls, it also results in reduced structural redundancy relative to Chilean walled buildings. It is therefore prudent to ensure that the mechanisms responsible for compression failures are understood.

This paper presents experimental results from two experimental programs, which were performed independently at two different universities after being developed to help better understand the compressive response of RC seismic-resisting wall boundary elements. The purpose is to assess the compressive performance of rectangular RC sections similar to, but not exact representations of, seismic-resisting wall boundary elements, in order to fill gaps in the available test data for such cases.

Both test programs used a series of rectangular RC specimens, with experimental parameters including transverse reinforcement ratio, transverse reinforcement detailing configuration, longitudinal reinforcement, tensile strain prior to peak compressive strength, and cross-sectional aspect ratio. Specimens were either tested in reversed cyclic or monotonic loading; some specimens were loaded in tension prior to commencing the cyclic or monotonic loading protocols. Nearly all of the test specimens meet the minimum ACI 318 (ACI 2014) detailing requirements (based on specified material properties) for boundary elements of special RC structural

[1]Postdoctoral Researcher, Univ. of Illinois Urbana-Champaign, 1325 Richelieu Ln., Houston, TX 77018 (corresponding author). E-mail: tswelt@gmail.com

[2]Associate Professor, Univ. of Chile, Beauchef 850, Santiago, Chile.

[3]Professor and Associate Head, Dept. of Civil and Environmental Engineering, Univ. of Illinois Urbana-Champaign, 3129B Newmark Civil Engineering Building, 205 N Mathews Ave., Urbana, IL 61801.

[4]Professor, Dept. of Civil and Environmental Engineering, Univ. of Washington, 214 B More Hall, P.O. Box 352700, Seattle, WA 98125.

[5]Earthquake Engineering Group Leader, Materials and Structural Systems Division, Engineering Laboratory, Gaithersburg, MD.

[6]Graduate Researcher, Univ. of Chile, Beauchef 850, Santiago, Chile.

Note. This manuscript was submitted on March 18, 2015; approved on August 29, 2016; published online on October 28, 2016. Discussion period open until March 28, 2017; separate discussions must be submitted for individual papers. This paper is part of the ***Journal of Structural Engineering***, © ASCE, ISSN 0733-9445.

walls, with additional specimens meeting and even exceeding the ACI 318-14 requirements for special boundary elements.

Existing Database of Rectangular RC Sections

Axial tests on reinforced concrete sections are common, however few of these focus on the performance of nonsquare, rectangular prisms. A brief summary of the relevant available tests is presented here. Mander et al. (1988a, b) investigated the effect of confinement on compressive response; those tests were constructed with large transverse reinforcement area ratios ranging from 3 to 6% (using ACI 318-14 for seismic detailing, typical ratios range between 0.5 and 2%). The test specimens performed exceptionally well and formed the basis of a commonly used confined concrete model. Acevedo et al. (2010), Creagh et al. (2010), and Chrysanidis and Tegos (2012) all used rectangular prisms to investigate the effect of tensile strain prior to compression loading on the compressive performance. The findings were consistent, indicating that large tensile strains (0.5% or larger) prior to compression loading can lead to a significant strength reduction, as much as 50%. Welt (2015) provides a detailed review of each of the mentioned tests programs, if more information is desired.

The two test programs presented in this paper complement and extend these prior tests. In particular, the test programs investigate (1) the amount of transverse reinforcement, (2) the configuration of the transverse reinforcement, including the impact of cross ties, (3) the restraint pattern, and (4) the type of loading (monotonic versus cyclic). These specimens are unique in their design and do not replicate prior tests. Both the University of Chile (UCh) and the U.S. Army Corps of Engineers Construction Engineering Research Laboratory (CERL) test programs focused on more practical levels of transverse reinforcement ratios, between 0.5 and 2.0%.

Overview of Seismic-Resisting Wall Design and Performance

Reinforced concrete seismic-resisting walls are composed of two subcomponents, the web and the boundary elements. The web resists the majority of the shear stresses (including load transfer by means of anchorage between the web transverse reinforcement at the boundary element), while the boundary elements resist the majority of the flexural demands; both subcomponents resist any additional axial stresses from gravity loads bearing on the wall. The flexural performance of the wall is therefore specifically related to the performance of the boundary elements. Fig. 1 shows the subcomponent breakdown of a seismic-resisting wall; the research presented in this paper concerns test specimens that are representative of seismic-resisting wall boundary elements.

In the U.S., the design rules for boundary elements within special RC seismic-resisting walls are provided by ACI 318-14. In cases where significant compressive strains are expected in the boundary element, ACI 318-14 requires the use of special boundary elements, which include more stringent detailing provisions. Boundary elements that meet the minimum ACI 318-14 requirements for special seismic-resisting walls, but do not meet the requirements prescribed for special boundary elements, are referred to as ordinary boundary elements in this paper. Boundary element detailing requirements are summarized in Fig. 2. The minimum transverse reinforcement ratio (defined in each direction as the area of steel divided by the core dimension times the transverse reinforcement spacing) shown in Fig. 2 applies to both special and ordinary boundary elements; for typical material properties of concrete ($f'_c = 30$ MPa) and reinforcing steel ($f_{y,t} = 420$ MPa), this

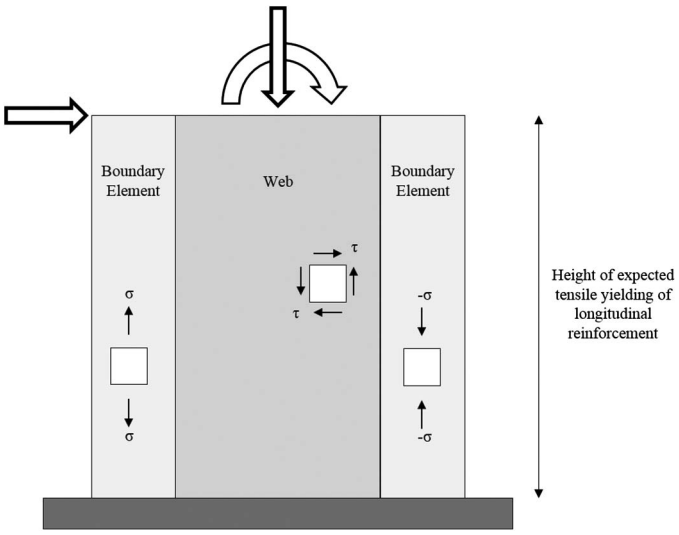

Fig. 1. Component breakdown of reinforced concrete seismic-resisting wall

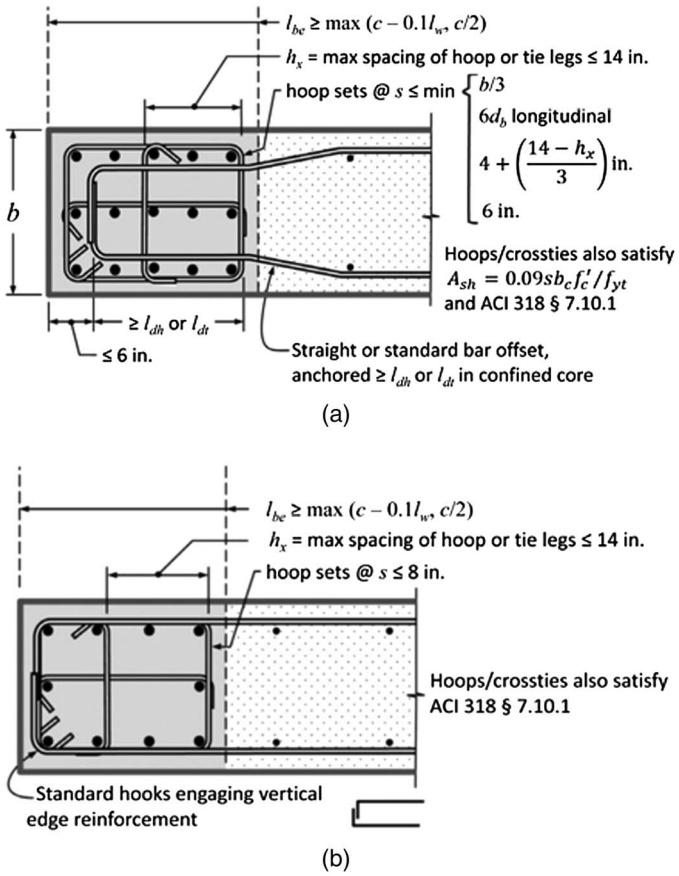

Fig. 2. Detailing requirements for (a) special boundary elements; (b) ordinary boundary elements per ACI 318-14 (image courtesy of Moehle et al. 2011)

results in a transverse reinforcement ratio of approximately 0.6% in each direction.

In Chile, design of boundary elements in seismic-resisting RC walls is currently governed by D.S. N°60 (MINVU 2010), which replaced the RC code NCh433.Of2008 (INN 2008) after the 2010

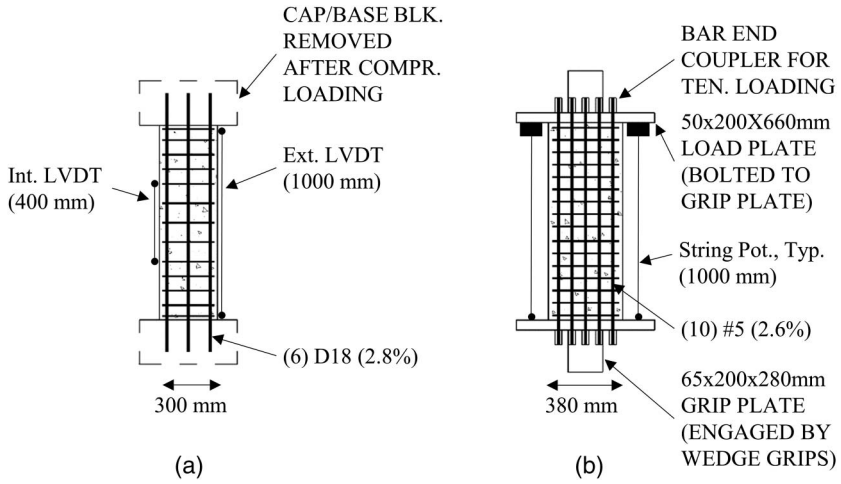

Fig. 3. Representative specimen elevations of (a) University of Chile Program; (b) CERL program

earthquake (Massone 2013). NCh433.Of2008 references the 2005 edition of ACI 318-05 (ACI 2005) for design and detailing of boundary elements in seismic-resisting walls. However, the majority of existing structures in Chile, including most of those damaged in the 2010 Maule earthquake, were designed based on NCh433.Of96 (INN 1996), which also provided requirements for the design of RC seismic-resisting walls (Massone et al. 2012). NCh433.Of96 references ACI 318-95 (ACI 1995), however seismic-resisting walls are exempted from special boundary detailing requirements by this code (boundary elements must only meet the requirements for ordinary boundary elements).

Analytical approaches for the axial strength and deformation capacity of boundary elements are typically based on the model proposed by Mander et al. (1988b). This model is a modification of the classic expression suggested by Richart et al. (1929), given in Eq. (1), which is based on the expected confining stress, f_l, in the core, assuming yielding of transverse reinforcement. In Eq. (1), f'_{cc} is the confined core concrete strength, f'_c is the unconfined concrete strength, ρ_s is the transverse volumetric reinforcement ratio, and f_{yt} is the yield strength of the transverse reinforcement. The tests by Richart et al. (1929) were performed on circular columns with either spiral confinement or various levels of hydrostatic active confinement.

$$f'_{cc} = f'_c + 4.1 f_l = f'_c + 4.1 \frac{\rho_s f_{yt}}{2} \tag{1}$$

Mander et al. (1988b) suggested that Eq. (1) underestimates the confined strength in specimens tested at lower (active) lateral pressures. In their model, a confinement effectiveness factor, k_e, which is based on arching effects in the longitudinal direction, is used to determine the confined strength. For rectangular sections, this factor is further based on arching effects in the cross section direction, which is a function of the number of longitudinal bars and transverse reinforcement spacing.

These adjustments were based on a suite of tests performed by Mander et al. (1988a) on rectangular RC specimens with transverse reinforcement ratios ranging between 2 and 3% in the direction of specimen thickness (the shorter cross-sectional dimension), and up to 6% in the direction of specimen width (the longer cross-sectional dimension). As previously noted, the ACI 318-14 minimum transverse reinforcement ratio for both ordinary and special boundary elements results in only about 0.6% in each direction.

Seismic-resisting wall design and analysis, as described previously, seek to produce walls with significant deformation capacity; yielding of the longitudinal reinforcement (and thereby energy dissipation) is preferred prior to significant loss in load carrying capacity as a result of compression (crushing, bar buckling) failure of the boundary element. However, many observations of RC seismic-resisting walls in buildings following recent earthquakes seem to indicate otherwise. Moehle et al. (2011) show representative examples of compression failures in seismic-resisting walls following the 2010 Maule earthquake in Chile, and Tellen et al. (2012) present representative examples of compression failures in seismic-resisting walls following the 2011 Christchurch earthquake in New Zealand. Furthermore, laboratory testing (Thomsen and Wallace 1994; Birely et al. 2012) has shown multiple instances of compression failures (such as bar buckling and crushing) prior to expected yielding of longitudinal reinforcement. These tests show that seismic-resisting walls that meet both the ordinary and special boundary element requirements can fail in bar buckling earlier than expected.

Experimental Program

The experimental data presented in this paper consists of selected specimens (those related to the parameters of interest) from two independently developed and executed testing programs. The first experimental program, performed at UCh, consists of 22 rectangular RC specimens; 17 of those specimens are presented in this paper. Specimens in this program were loaded in monotonic compression, with some specimens loaded in tension to a specific tensile strain prior to monotonic compression testing. The second experimental program, performed through the University of Illinois at CERL, consists of 18 specimens loaded in either monotonic compression or reversed cyclic tension and compression; 16 of those specimens are presented in this paper. The cyclic loading protocol consisted of two cycles to each new average vertical strain value, including 0.15, 0.3, 0.6, and 1.0%, and then intervals of 0.5% from that point forward.

Specimen elevations are shown for the UCh and CERL testing programs in Figs. 3(a and b), respectively. All specimens were 1.0 m in height, with the exception of specimens P9 and P11, which were 1.6 m in height. As shown in Fig. 3(a), the transverse reinforcement in the UCh tests was more closely spaced near

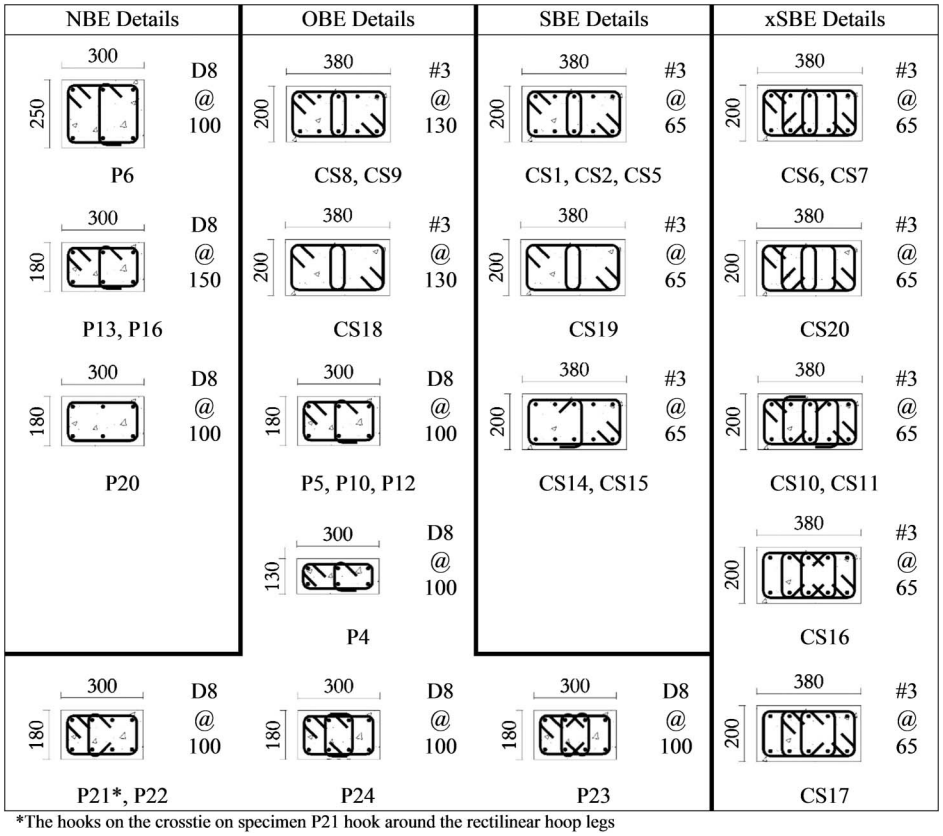

Fig. 4. Specimen cross section designs

the top and bottom of those specimens, with the intent of creating a failure near midlength.

In the UCh testing program, specimens were cast horizontally; for specimens intended for tensile loading, the longitudinal rebar extended beyond the forms for use in the concrete cap and base blocks. Tensile loading was applied prior to monotonic compression using hydraulic jacks spanning between the concrete cap and base blocks. After tension loading was applied, the jacks were removed and the concrete cap and base blocks were sawn off. Specimens intended for compression only were cast vertically, however without any cap or base block. All specimens were vertically loaded in compression using a uniaxial testing frame. No positive connection was provided between the testing machine and the specimens, and therefore relative rotation at the specimen boundaries was permitted during compression loading, although the loading plates in the uniaxial testing machine were not able to rotate and therefore tended to minimize such relative end rotation under significant compression loading.

In the CERL testing program, specimens were cast vertically. The longitudinal reinforcement extended beyond the concrete. The structural steel loading test fixtures were affixed to the rebar protrusions using Dayton Superior D260 BarLock mechanical couplers (Dayton Superior, Miamisburg, Ohio), as shown in Fig. 3(b). Axial tension and compression loading were accomplished using a uniaxial test machine with wedge grips that engaged the couplers through a steel plate bracket assemblage. The plate bracket is bolted together with three bolts aligned along the centerline of the length of the specimen cross section. The bolted nature of this connection allows for relative rotation in the out-of-plane direction at each end of the specimen. However, analysis of the displacement data (Welt 2015) shows that the deformation was relatively uniform over the specimen cross section. Uniform loading was desired (and has been assumed elsewhere in the data analysis), which is confirmed by this finding.

The loading and boundary conditions in these tests do differ slightly from those in a boundary element within a seismic-resisting wall. In the tests, uniform loading is applied to the bars (CERL) or the concrete (UCh). In the elastic range, the horizontal axial displacement profile of a seismic-resisting wall is linear, whereas the horizontal axial displacement profile in the specimens is approximately uniform. However, tests of seismic-resisting walls indicate that at drifts resulting in cover damage, the horizontal axial displacement across the boundary element is more uniform (Birely 2012). As such, this experimental approximation of the compressive performance of a boundary element is appropriate.

Specimens in both experimental programs are classified into four individual transverse detailing classes, based on ACI 318-14 requirements for length (§18.10.6.5), thickness (§18.10.6.4a,b), horizontal spacing of longitudinal bars (§18.7,5,2e), area of transverse reinforcement (§18.10.6.4f), and crossties (§25.3.2); these classes include, noncompliant boundary elements (NBE), ordinary boundary elements (OBE), special boundary elements (SBE), and enhanced special boundary elements (xSBE). Fig. 4 shows the cross-sectional variations within each detail class. The detail classification is selected for each specimen based on the design material properties, not on the actual measured properties. Overstrength of materials, as would be typical in design and construction practice, is not considered in determining the boundary element detail classification. Furthermore, the UCh specimens that are considered ordinary boundary elements, per ACI 318-14 transverse reinforcement spacing limit of one-third the thickness, met all other SBE requirements.

Table 1. Specimen Design and Testing Parameters

Specimen	f'_c[a] (MPa)	H_w/t_w	L_w/t_w	s/d_b	$\rho_{l,be}$ (%)	ρ_x (%)	ρ_y (%)	ε_{t0} (%)	Prot.	f'_{cc}/f'_c predicted[b]	f'_{cc}/f'_c measurements	$\bar{\varepsilon}_{\text{predicted}}$[c] (%)	$\bar{\varepsilon}_{\text{measured}}$ (%)
University of Chile Program (unconfined—P1:P3, P7, P8; NBE—P13:P20; OBE—P4:P6, P10, P11, P21:P24)													
P1	39	7.7	2.3	—	3.9	—	—	0	Mon	—	—	0.4	0.4
P2	39	5.5	1.7	—	2.8	—	—	0	Mon	—	—	0.4	0.6
P3	39	4.0	1.2	—	2.0	—	—	0	Mon	—	—	0.4	0.6
P4	39	7.7	2.3	5.6	3.9	0.77	0.50	0	Mon	1.1	1.3	2.3	0.6
P5	39	5.5	1.7	5.6	2.8	0.56	0.50	0	Mon	1.2	1.3	2.0	0.6
P6	39	4.0	1.2	5.6	2.0	0.40	0.50	0	Mon	1.2	1.3	1.7	1.0
P7	39	5.5	1.7	—	2.8	—	—	1	Mon	—	—	0.4	0.4
P8	39	5.5	1.7	—	2.8	—	—	2	Mon	—	—	0.4	0.4
P10	39	5.5	1.7	5.5	2.8	0.56	0.50	2	Mon	1.2	1.0	2.0	0.5
P11	39	8.9	1.7	5.5	2.8	0.56	0.50	2	Mon	1.2	1.2	2.0	0.6
P13	39	5.5	1.7	8.3	2.8	0.37	0.34	0	Mon	1.1	1.2	1.5	0.6
P16	39	5.5	1.7	8.3	2.8	0.37	0.34	2	Mon	1.1	0.9	1.5	0.4
P20	39	5.5	1.7	8.3	2.8	0.56	0.34	0	Mon	1.2	1.0	1.7	0.7
P21	39	5.5	1.7	5.6	3.8	0.56	0.50	0	Mon	1.2	1.3	2.0	1.1
P22	39	5.5	1.7	5.6	3.8	0.56	0.50	0	Mon	1.2	1.1	2.0	1.3
P23	39	5.5	1.7	5.6	3.8	0.56	0.67	0	Mon	1.3	1.1	2.2	1.5
P24	39	5.5	1.7	5.6	3.8	0.56	0.67	0	Mon	1.3	1.3	2.2	1.6
CERL Program (OBE—CS8, CS9, CS18; SBE—CS1, CS2, CS5, CS12:CS15, CS19; xSBE—CS6, CS7, CS10, CS11, CS16, CS17, CS20)													
CS1	27	5.0	1.9	4.0	2.6	1.10	1.17	0	Cycl	1.9	1.4	3.6	2.3
CS2	27	5.0	1.9	4.0	2.6	1.10	1.17	5	Cycl	1.9	0.7	3.6	1.8
CS5	28	5.0	1.9	4.0	2.6	1.10	1.17	0	Mon	1.8	1.5	3.6	2.0
CS6	29	5.0	1.9	4.0	2.6	1.10	1.76	0	Cycl	1.9	2.0	4.4	4.1
CS7	29	5.0	1.9	4.0	2.6	1.10	1.76	0	Mon	1.9	1.9	4.4	3.7
CS8	29	5.0	1.9	8.0	2.6	0.55	0.59	0	Cycl	1.3	1.2	2.0	0.7
CS9	29	5.0	1.9	8.0	2.6	0.55	0.59	0	Mon	1.3	1.3	2.0	0.6
CS10	27	5.0	1.9	4.0	2.6	1.10	1.76	0	Cycl	2.0	1.5	4.4	2.5
CS11	27	5.0	1.9	4.0	2.6	1.10	1.76	0	Mon	2.0	1.4	4.4	2.6
CS14	28	5.0	1.9	4.0	2.6	1.10	0.88	0	Cycl	1.7	1.1	3.2	0.9
CS15	28	5.0	1.9	4.0	2.6	1.10	0.88	0	Mon	1.7	1.2	3.2	1.2
CS16	33	5.0	1.9	4.0	2.6	1.10	1.47	0	Cycl	1.8	1.6	4.0	2.5
CS17	33	5.0	1.9	4.0	2.6	1.10	1.47	0	Cycl	1.8	1.7	4.0	2.5
CS18	34	5.0	1.9	8.0	0.0	0.55	0.55	0	Mon	1.3	1.2	2.0	0.7
CS19	34	5.0	1.9	4.0	0.0	1.10	1.17	0	Mon	1.8	1.5	3.6	1.8
CS20	34	5.0	1.9	4.0	0.0	1.10	1.76	0	Mon	1.9	1.5	4.4	2.2

[a]Test day measured cylinder compressive strength.
[b]Mander et al. (1988a).
[c]Scott et al. (1982).

Table 2. Steel Reinforcement Material Properties

	Transverse reinforcement		Longitudinal reinforcement	
Test program	f_y (MPa)	f_u (MPa)	f_y (MPa)	f_u (MPa)
UCh	495	700	482	690
CERL	470	690	545	675

Pertinent test parameters across both programs include tensile strain, cross-sectional aspect ratio (length-to-thickness ratio), height-to-thickness ratio, transverse reinforcement ratio, cross-sectional detailing configuration, and longitudinal reinforcement. Table 1 lists the details of all specimens from each program. UCh tests are denoted P#, and CERL tests are denoted CS#. The UCh tests occurred within approximately two months of casting, with a single batch of cylinder tests (at 28 days) used to determine the unconfined strength for all specimens. Cylinders were tested within one day of specimen testing for all of the CERL tests. Specimens P1–P3, P7, and P8 are considered unconfined, as no transverse steel was installed in the interior region of those specimens. Specimens CS18–CS20 were constructed without longitudinal reinforcement. In Table 1, t_w is the specimen thickness, L_w is the cross-sectional length, H_w is the specimen height, s is the transverse reinforcement spacing, d_b is the longitudinal bar diameter, $\rho_{l,be}$ is the longitudinal reinforcement ratio, and ρ_x and ρ_y are the transverse reinforcement ratio perpendicular and parallel to the thickness, respectively. Significant tensile strain prior to either cyclic or monotonic loading is denoted by ε_{t0}. Also, the measured and predicted peak confined strengths and strains are shown, which are described later in the text.

Transverse reinforcement material strengths are shown in Table 2. The steel specifications for the CERL tests were ASTM A615 Gr. 60 (ASTM 2014a) and ASTM A706 Gr. 60 (ASTM 2014b) for the longitudinal and transverse reinforcement, respectively. The steel specification for the UCh tests was Acero (steel) A63-42H (INN 2006) for both the longitudinal and transverse reinforcement. The specifications for A63-42H are similar (in terms of strength and elongation requirements) to those of ASTM A615 Gr. 60.

Axial displacement was measured using two different methods in the UCh tests by means of LVDTs. The LVDTs that measured the displacement over the entire height of the specimen are referred to as external, whereas the LVDTs that measured the displacement over a smaller, middle region of the specimen (400 mm) are

Fig. 5. Final damage states of monotonic tests of various detail classes: (a) unconfined–P2; (b) NBE–P20; (c) OBE–CS9; (d) SBE–CS5; (e) xSBE–CS7

referred to as internal; this internal length is the same as the study region that was reinforced to meet the design classification, as noted in Fig. 3(a).

The average strains presented in this paper are based on the measured displacements using the external LVDTs. In the CERL tests, the axial displacement used to quantify the average strain was measured using a pair of string potentiometers on either end of the specimen that span between the loading brackets shown in Fig. 3(b). In tension, a small displacement error occurs due to the elongation of the rebar over the thickness of the bearing plate portion of the steel bracket, which is captured by the string potentiometers that span between the brackets. The maximum observed tensile strain is approximately 5%, which is equivalent to a total of about 0.25 mm of rebar elongation over the thickness of each bracket. This amounts to 1% of the total tensile deformation, and is therefore considered negligible. This error does not occur at all during compression loading, as the steel bracket bears directly on the specimen.

The average strain was calculated as the displacement measurement divided by gage length. Using the entire specimen length provided an approximately equivalent method for both test programs and ensured that the entire damaged region was captured by the strain measurement.

The average measured deformation capacity of the test specimens, $\varepsilon_{\text{measured}}$, is calculated as the measured strain at 30% loss in strength. This definition is based on the observed damage mode (bar buckling) that is consistently followed throughout both test programs by a sharp drop off in load carrying capacity. The predictive model (Mander et al. 1988b) assumes that loss in strength is associated with the onset of transverse hoop fracture; such behavior did not occur in any of the tests in either program, nor those in the previous tests discussed (aside from Mander et al. 1988a). The strain corresponding to bar buckling in reinforced concrete is difficult to accurately predict, and therefore the definition of 30% strength loss provides a consistent means with which to describe the strain at which the specimen no longer exhibits load carrying capacity.

Load was measured by means of a standard load cell in the uniaxial test frame in both experimental programs. To better understand the performance of the concrete, the contribution of the longitudinal steel was subsequently removed from the load response. Strain in the longitudinal reinforcement was measured in both experimental programs using strain gauges, from which the stress was calculated using an elastoplastic model; this assumption was reasonable for rebar in compression over the range of compression strains of interest. Once the contribution of the steel was removed, the remaining load was considered to be the contribution of the concrete, P_c. Results presented in this paper are based on the normalized stress in the core concrete, which was calculated by dividing the contribution of the concrete, P_c, by the core concrete area, A_{core}. The core area, A_{core}, was calculated as the area bounded by the centerlines of the peripheral longitudinal reinforcement, as recommended by Mander et al. (1988a).

Experimental Results

Fig. 5 shows the observed final damage states for representative monotonic specimens from each of the four detailing classes (NBE, OBE, SBE, xSBE), as well as an unconfined specimen. The discussion that follows is specific to the final damage state; spalling and crushing consistently occurred prior to this point. There is a clear distinction in the failure mode of each detail class. The unconfined specimen (P2) and the NBE specimen (P20) failed due to a combination of concrete crushing and bar buckling at approximately 0.5% average strain. In the OBE specimen, bar buckling was also observed, however, the specimen also buckled out-of-plane (as shown in Fig. 5), again at approximately 0.5% average strain. The damage observed in the SBE specimen is similar to the OBE specimen, however, the SBE specimen failed in bar buckling at approximately 2.0% average strain. The damage is relatively well distributed in the xSBE specimen along its height; the xSBE specimen eventually failed in bar buckling at approximately 3.5% average strain.

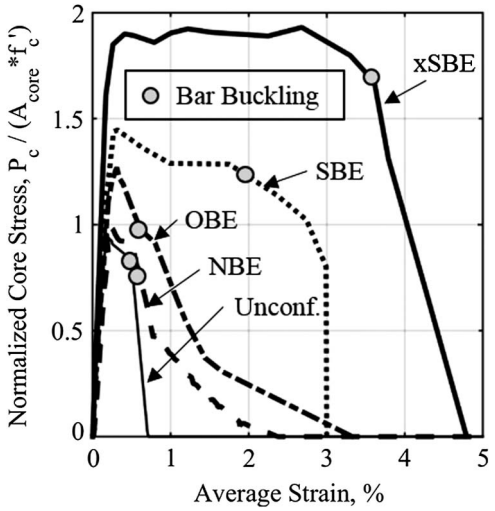

Fig. 6. Compressive response of various detail classifications: xSBE–CS7; SBE–CS5; OBE–CS9; NBE–P5; unconfined–P2

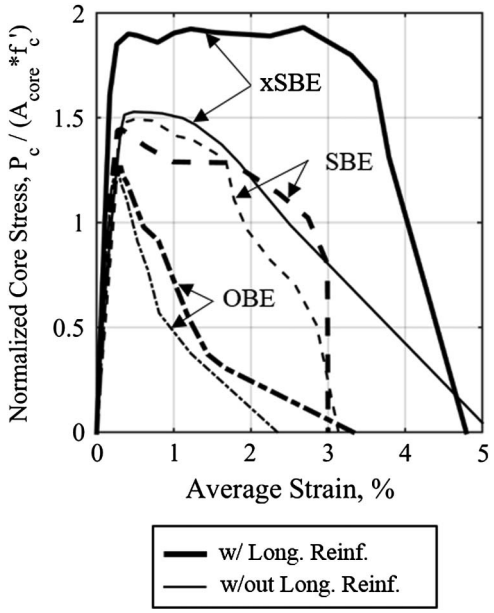

Fig. 7. Comparison of specimens with and without longitudinal reinforcement: xSBE–CS7 and CS20; SBE–CS5 and CS19; OBE–CS9, CS20

The normalized stress-strain behaviors of the specimens from Fig. 5 are shown in Fig. 6. As discussed, the normalized stress was calculated as the contribution of the concrete, P_c, divided by the product of cylinder strength and core area. In the unconfined case, the core area was simply taken as the gross area. As shown, the NBE and OBE specimens exhibited similar strength and strain capacity as compared with the unconfined specimen, however, these specimens did exhibit improved load carrying capacity (albeit after a 30% reduction in strength). In fact, substantial increases in confined strength and deformation capacity were only realized in the SBE specimens, and most notably in the xSBE specimens (in which each longitudinal bar was restrained in each orthogonal direction by a rectangular hoop).

Influence of Detailing Configuration

Stability of Longitudinal Reinforcement

Strength loss on the order of 30% was consistently realized in the test specimens along with the occurrence of either longitudinal bar buckling or sectional buckling, as indicated in Fig. 6. These observations indicate that the stability of the longitudinal bars is directly related to deformation capacity.

Fig. 7 shows the compressive response of otherwise identical specimens, with and without longitudinal reinforcement, for OBE, SBE, and xSBE detailing classifications. There was little or no difference in compressive response with and without longitudinal reinforcement, with the exception of the xSBE case (where all longitudinal bars are restrained within a rectangular hoop), as shown in Fig. 7.

In addition to indicating that unbuckled longitudinal bars contribute to confinement, this further supports the conclusions of Fig. 6, where confined strength and deformation capacity are enhanced (by approximately 30 and 100%, respectively) if every longitudinal bar is restrained.

Configuration of Transverse Reinforcement

The use of crossties in place of rectangular hoops to restrain noncorner longitudinal bars is commonplace in the RC construction industry for ease of installation. This practice is permitted by ACI 318-14 as long as at least one end of the crosstie terminates in a 135° hook of 6 times the bar diameter, or a minimum of 75 mm.

Both of the experimental programs reported here include specimens designed to investigate the effectiveness of crossties, in both type and quantity. As shown in Fig. 4, specimens were cast with different combinations of either 90°–135° or 135°–135° crossties. The UCh specimens aim to quantify the effect of different configurations of crossties, whereas the CERL specimens aim to compare the effectiveness of crossties versus rectangular hoops. Rectangular hoop implies that the hoop is closed by hooks, and does not consist of crosstie legs. Crosstie hooks on the UCh specimens have extensions of 90 mm, or approximately 11 times the bar diameter; CERL specimens have extensions of 60 mm, or 6 times the bar diameter.

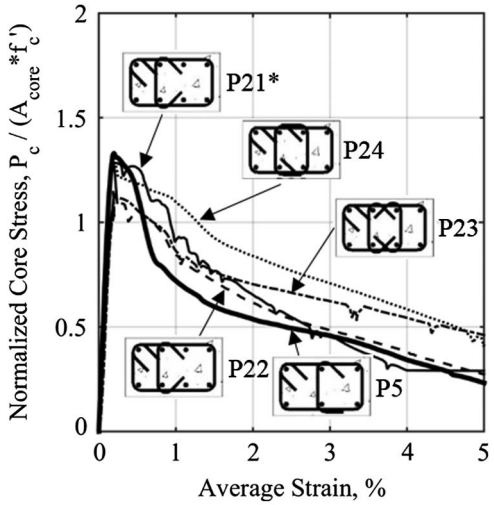

Fig. 8. Effectiveness of various crosstie configurations for ordinary boundary elements

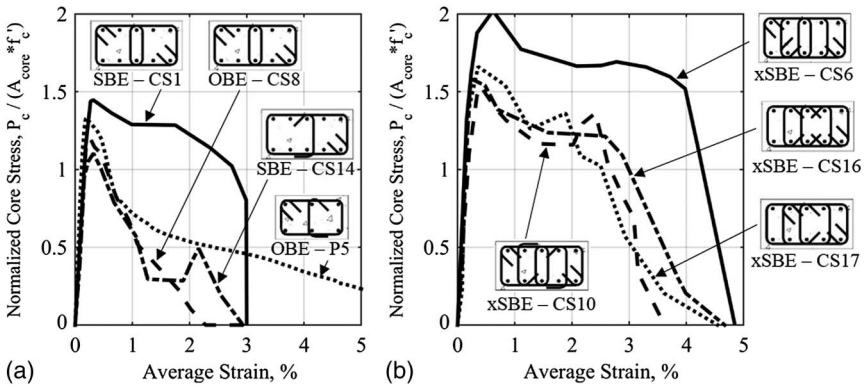

Fig. 9. Comparison of crossties versus rectangular hoops for (a) special and ordinary boundary elements; (b) enhanced special boundary elements

Fig. 10. Final damage state of a special boundary element: (a) with 90°–135° crossties (Specimen CS14); (b) with all rectangular hoops (Specimen CS1)

Tests in the CERL program are designed at 2/3-scale (with respect to a medium-rise RC wall building in the U.S. where the wall thickness would range between about 200 to 600 mm), and therefore the absolute minimum hook extension required per ACI 318-14 (of 75 mm) was taken as 50 mm; the UCh tests are full-scale.

Fig. 8 shows the compressive response of monotonic tests within the UCh program; all specimens shown are considered to be OBEs with a transverse reinforcement ratio of approximately 0.5–0.6% in each direction. The results do not show a significant variation in performance, although some specific observations can be made. A comparison of specimen P5 with specimens P22–P24 shows that inclusion of more longitudinal reinforcement (as in specimens P22–P24) may result in a slightly enhanced deformation capacity (as compared with that of specimen P5), however this could also be attributed to the change in confining steel and is therefore inconclusive. Specimen P21 is constructed with the crosstie hooks wrapping around the main rectangular hoop, which appears to be slightly beneficial in terms of peak strength, as compared with specimen P22 in which the crossties are stacked on the hoops (common practice).

The effectiveness of crossties to adequately restrain longitudinal reinforcement in a manner similar to that of rectangular hoops is presented in Fig. 9. The OBE and SBE specimens are shown in Fig. 9(a), and the xSBE specimens are shown in Fig. 9(b). In this figure, although specimens CS8 and P5 are both OBE, specimen P5 appears to perform better.

The crossties do not appear to have an effect on the response of the OBE specimens as compared with the rectangular hoops. Reductions in peak strength and deformation capacity are observed in both the SBE and the xSBE specimens constructed with crossties as compared with those constructed with only rectangular hoops. This result is consistent regardless of the shape of the crosstie, as supported by Fig. 8. The result is also consistent for specimen CS17, which is constructed with two rectangular hoops and a single crosstie in the middle. This indicates that using crossties to anchor a high aspect ratio rectangular hoop may not provide equivalent intermediate longitudinal bar restraint as compared to using rectangular hoops for anchorage. As shown in Fig. 9(b), crossties with 135°–135° standard hooks do not appear to provide any additional benefit as compared to crossties with 90°–135° standard hooks.

The observed damage in these tests further points to the ineffectiveness of crossties to adequately restrain the longitudinal reinforcement. Fig. 10(a) shows the final damage zone of a specimen with crossties, whereas Fig. 10(b) shows the final damage zone of a specimen constructed with all rectangular hoops. As shown, the core appears to maintain integrity in the specimen with overlapping rectangular hoops, whereas the specimen with crossties shows core-crushing damage in addition to the crossties pulling out of the core (resulting in an unrestrained longitudinal bar). This behavior was typically observed near the time of bar buckling, and thus was likely related.

These results indicate a clear distinction in the performance of specimens constructed with crossties used in place of rectangular

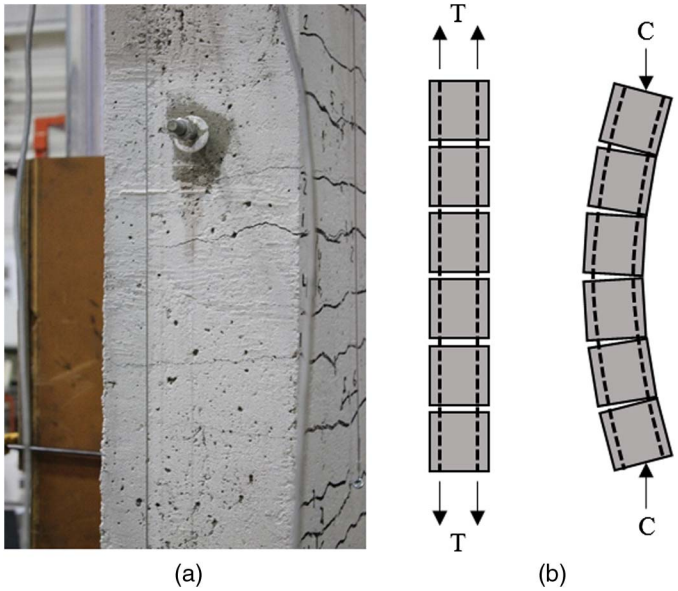

Fig. 11. (a) Specimen CS2 at neutral after 5.0% tensile strain; (b) instability of sections subjected to tensile strain

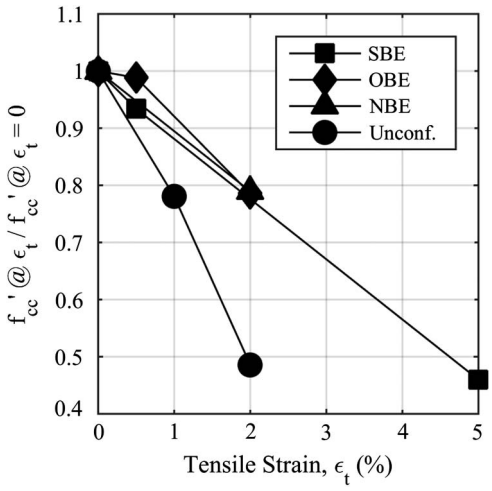

Fig. 12. Influence of tensile strain on the confined core strength

hoops. Specifically, crossties do not appear to provide adequate (as defined by specimens with rectangular hoops) longitudinal bar restraint, which may lead to premature compressive failure (reduction in deformation capacity) and reduce the effectiveness of confining steel to increase the confined strength of the concrete core. This reduction in effectiveness is not as apparent in the OBE specimens, however none of the specimens within this detailing classification showed any significant deformation capacity that could be jeopardized by the use of crossties.

Influence of Tensile Strain

Paulay and Priestley (1993) suggest that tensile strain prior to compression loading (called tensile prestrain) affects the confined concrete core strength. Specifically, they suggest that nonuniform yielding of individual curtains of reinforcement results in nonuniform crack closure across the section thickness, which can cause instability and therefore a reduction in capacity. To further explore this phenomenon, both experimental programs investigated the effects of an initial tensile strain excursion prior to the start of either monotonic or cyclic loading for detailing classes ranging from unconfined to enhanced special boundary elements. The tension limits employed during the UCh and CERL tests are based on analyses of wall response (Birely et al. 2012) and other prior research on rectangular reinforced concrete specimens (Acevedo 2010; Creagh et al. 2010) indicating larger tensile strains may negatively impact the compressive response.

Fig. 11(a) shows a photo of specimen CS2 in the neutral displacement position (i.e., the actuator zero-displacement position) after a tensile prestrain excursion to approximately 5.0%; Fig. 11(b) depicts the scenario suggested by Paulay and Priestley (1993). The observed damage at the neutral displacement position indicates that, at the initiation of compression loading, the specimen is likely to experience P-δ effects similar to those shown in Fig. 11(b). Fig. 12 shows the confined strength of specimens of various boundary element detailing classes, for a range of tensile prestrains imposed prior to reaching the compressive capacity, normalized by the confined strength of nominally identical specimens not exposed tensile prestrain.

The maximum tensile prestrain imposed on an xSBE specimen was 0.5%, which resulted in negligible effects on the compressive response; for clarity and efficiency, these results are not shown. The reduction in confined strength appears similar for all other detailing classes, with tensile prestrain more significantly (as shown by the steeper slope in the figure) affecting unconfined sections. For the OBE and SBE specimens, tensile prestrains of approximately 0.5% produced at most a 5% reduction in confined strength, while tensile prestrains of 2.0 and 5.0% produced approximately 20 and 50% reductions in confined strength, respectively. In the unconfined case, tensile prestrains of 1.0 and 2.0% produced reductions in confined strength of approximately 20 and 50%, respectively.

Influence of Cross-Sectional Aspect Ratio

The UCh program includes specimens over a range of cross-sectional aspect ratios (section length divided by section thickness, L_w/t_w), detailed as either OBEs or unconfined. Specimens P1–P3 are unconfined specimens, and have cross-sectional aspect ratios of 2.3, 1.7, and 1.2, respectively. Specimens P4–P6 are detailed as OBEs, and have similar cross-sectional aspect ratios to specimens P1–P3. The transverse reinforcement in specimens P4–P6 is of the same configuration and spacing, resulting in a variation of the actual transverse reinforcement ratio in each direction for each specimen (as indicated in Table 1). The thickness of the specimen is the only parameter that changes in these cases.

Fig. 13(a) shows the normalized stress versus average strain of the OBE specimens (P4, P5, and P6), while Fig. 13(b) shows the normalized stress versus average strain of the unconfined specimens (P1, P2, and P3). In both detailing cases, the confined core strength is weakest for the specimens with a cross section aspect ratio of 2.3, by at least 10% in each case. Little difference is observed in specimens with aspect ratios of either 1.7 or 1.3. The characteristic trend of this portion of the study, although minor, lies in the observed average strain response. In the case of the OBE specimens, the specimen with a cross-sectional aspect ratio of 1.2 (nearly square) exhibits somewhat of an enhanced deformation capacity following the peak stress.

These results indicate that, for OBEs, the compressive response is not affected by cross-sectional aspect ratio. This is likely a result of the specimens with higher cross-sectional aspect ratios having

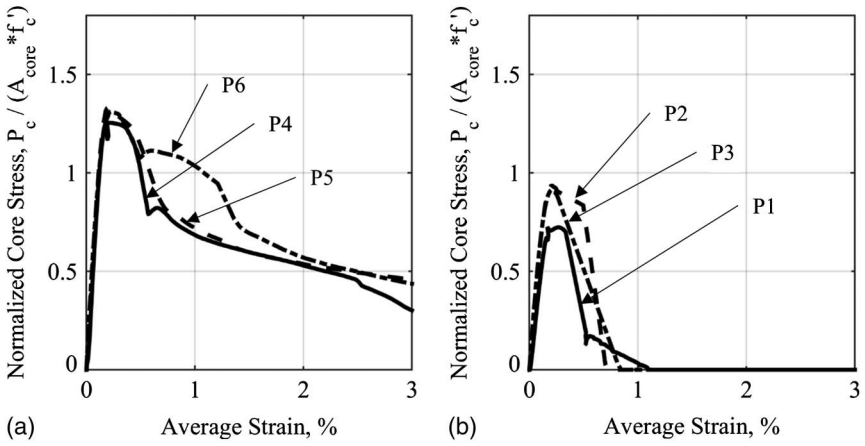

Fig. 13. Effect of cross-sectional aspect ratio for (a) ordinary boundary elements; (b) unconfined sections

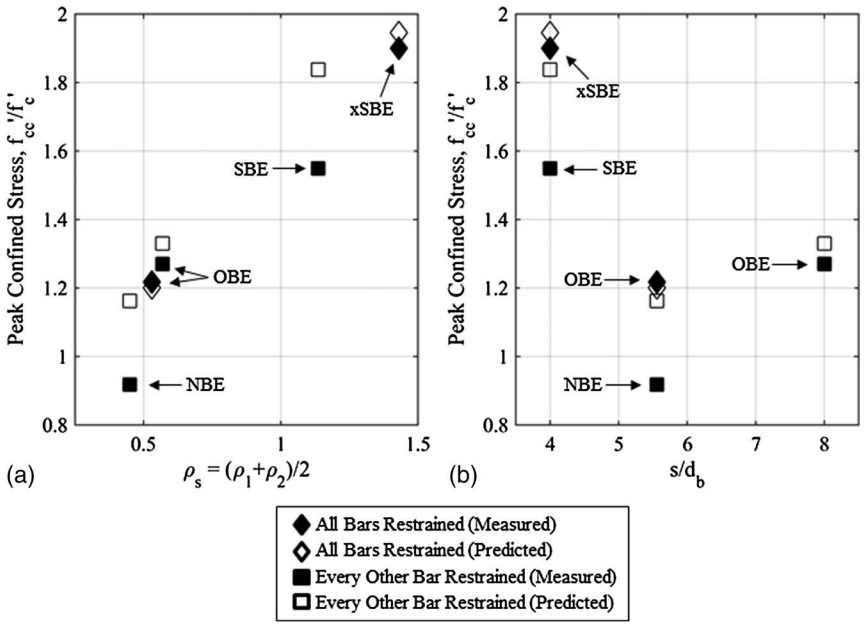

Fig. 14. Comparison of measured versus predicted strength for (a) transverse reinforcement ratio; (b) tie spacing to bar diameter

higher transverse reinforcement ratios. Because of the changing transverse reinforcement ratios between these specimens, it is difficult to clearly establish the effects of cross-sectional aspect ratio in OBE specimens. It is not immediately clear if the cross-sectional aspect ratio would have as negligible an effect on sections detailed as SBEs or xSBEs.

Comparisons with Existing Predictive Modeling Techniques

The previously discussed model suggested by Mander et al. (1988b) is based on tests performed with rectangular RC sections similar to those presented in this paper, however, with significantly larger transverse reinforcement ratios (on the order of 3–6%). It may therefore be prudent to compare the performance of the test specimens presented in Fig. 6, which have transverse reinforcement ratios more indicative of modern design and construction, with the predicted behavior based on the model suggested by Mander et al. (1988b). Table 1 shows the measured and predicted (Mander et al. 1988b) peak confined strengths and the measured and predicted (Scott et al. 1982) deformation capacities for all specimens.

Fig. 14 shows a comparison between the measured and predicted normalized confined strengths based on the Mander model. In Fig. 14(a), normalized peak confined stress is shown as a function of transverse reinforcement ratio, whereas in Fig. 14(b) confined stress is shown as a function of the ratio of horizontal spacing of confining steel to diameter of the longitudinal bars, s/d_b. Distinction is made between specimens with every longitudinal bar restrained and those with every other bar restrained. Both measured and predicted confined strength appear to increase steadily with the transverse reinforcement ratio, as shown in Fig. 14(a); confined strength generally appears to decrease as a function of the ratio, s/d_b, as shown in Fig. 14(b). The accuracy of the predictive model is clearly related to the amount of longitudinal bars that are restrained within the cross section. As shown in Fig. 14(b), the predictive model overestimates the confined strength of specimens with a value of s/d_b of 6 or less (one of the ACI 318-14

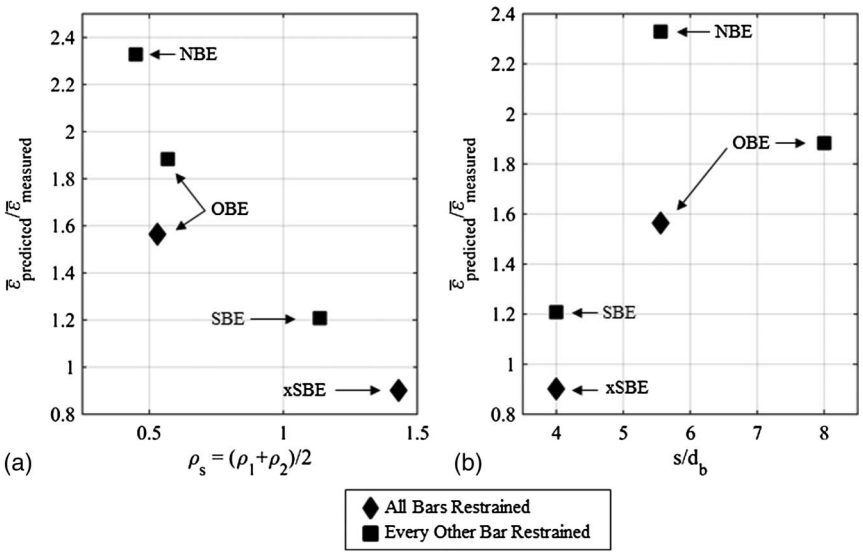

Fig. 15. Comparison of measured versus predicted deformation capacity for (a) transverse reinforcement ratio; (b) tie spacing to bar diameter

requirements for special boundary elements) that have every other longitudinal bar restrained.

Fig. 15 shows the overestimation of deformation capacity by the predictive model (Mander et al. 1988b) as a function of (1) transverse reinforcement ratio, and (2) the ratio s/d_b. Specimens with each longitudinal bar restrained are distinguished from those with every other bar restrained. In Fig. 15, the predicted ultimate average strain, $\bar{\varepsilon}_{predicted}$, is calculated as the estimated transverse hoop fracture strain (Scott et al. 1982) minus the strain associated with the predicted peak confined strength using the Mander model. The predictive model assumes that strain at failure of the confined concrete is controlled by transverse hoop fracture, and therefore is a reasonable estimate as to the extent (in terms of strain) of the predicted load carrying plateau.

Measured deformation capacity of the test specimens, $\bar{\varepsilon}_{measured}$, is calculated as the strain at 30% strength loss minus the strain at the peak capacity. This definition is based on bar buckling consistently marking the point at which the load carrying capacity experiences a sharp drop off. Throughout both test programs, this damage mode consistently occurred near a 30% loss in strength, indicating that compressive capacity is linked to the onset of bar buckling. As previously discussed, the deformation capacity in the predictive model is based on the onset of hoop fracture, however none of the specimens in either program exhibited this behavior. Therefore, use of a damage-based approach (30% strength loss) to determining the experimental deformation capacity is consistent with the approach of the predictive model.

Fig. 15(a) indicates that the predictive Mander model overestimates the deformation capacity of OBE and NBE specimens, in some cases by over twice the measured capacity. The model is slightly more accurate for SBE specimens, overestimating the deformation capacity by approximately 20%. The predicted deformation capacity of the xSBE specimens is within 5%, and is actually an underestimate. This accuracy of predicting the xSBE response is not unexpected, as those specimens are near to the lower limit of transverse reinforcement in the specimens used by Mander et al. (1988a) to develop the predictive model. The accuracy of the predictive model is related to the number of longitudinal bars restrained in the cross section; in terms of s/d_b, the overestimation is most severe for specimens with every other bar restrained, at just under the maximum ACI 318-14 limit (of 6) for special boundary elements.

Conclusions

This paper has presented experimental results from two independently developed and executed testing programs composed of rectangular RC specimens subjected to axial loading. The specimens fill a significant gap in existing data for rectangular sections simply meeting the minimum ACI 318-14 requirements for ordinary and special boundary elements of special RC seismic-resisting walls. The following trends have been observed:

- Boundary elements meeting the minimum special boundary element and ordinary boundary element provisions of ACI 318-14 fall short of the predicted (Mander et al. 1988b) deformation capacity. The expected behavior of confined RC components in flexural systems is to sustain the compressive force and displacement demands in order to permit cyclic yielding of the system, thereby promoting a tension-controlled failure. Only the xSBE specimens with closed hoops maintained load carrying capacity (with a reduction of less than 10% from peak stress) at compressive strains exceeding 1% and therefore would be best suited to achieve this objective.
- The use of crossties reduces the strength and deformation capacity of rectangular RC sections. Crossties, either with 90°–135° or 135°–135° hooks, do not appear to provide a significant restraint against longitudinal bar buckling. This result is consistent throughout the various detailing configurations tested, indicating that crossties and rectangular hoops may not be interchangeable, as prescribed by the ACI 318-14 requirements.
- Test results indicate that the stability of longitudinal reinforcement is directly related to the deformation capacity of rectangular RC sections. Comparisons of identical specimens with and without longitudinal reinforcement show increased deformation capacity in the confined core only in the case where each longitudinal bar is restrained in each direction by a rectangular hoop.
- Tensile strain prior to reaching the compressive capacity affects the strength of confined concrete in rectangular sections. Specifically, tensile strains of 2.0 and 5.0% result in compressive strength reductions of 20 and 50%, respectively, in ACI 318-14 compliant ordinary and special boundary element specimens. This finding is consistent with other previous tests.
- The strength and deformation capacity of ordinary and special boundary elements meeting the minimum ACI 318-14 requirements for special seismic-resisting walls appear to be

overestimated by a popular existing predictive model. Enhanced special boundary element specimens, with all longitudinal reinforcement restrained by legs of rectangular hoops in each direction, represented the only specimens with responses similar to what would be predicted by that model.

Acknowledgments

The work completed at the UCh was financially supported by InnovaChile-Corfo under Grant No. 10CREC. The contribution of the Chilean Concrete and Cement Institute (ICH) through Mr. Augusto Holmberg is also greatly acknowledged. The work completed at the U.S. Army Corps of Engineers Construction Engineering Research Laboratory (CERL) is part of a continuing study financially supported by the National Earthquake Hazards Reduction Program (NEHRP) at the National Institute of Standards and Technology. The authors would like to specifically recognize Dr. Steven McCabe (NEHRP) for his contributions to this research project including deft oversight, technical insights and valuable feedback. The idea and value of this research resulted from Dr. McCabe's continuous leadership in earthquake engineering. The authors would like to acknowledge the contributions from students including Mr. Jesús Núñez (UCh), Mr. Ahraaz Qureishi (CERL), and Mr. Alex Hargus (CERL) for their assistance in the development, construction, and testing of the specimen results presented in this paper.

Notation

The following symbols are used in this paper:

A_{core} = confined core area of cross section;
A_g = gross area of cross section;
d_b = longitudinal bar diameter;
f_c = stress in concrete at a given location;
f'_c = test-day cylinder compressive strength of concrete;
f'_{cc} = confined core concrete compressive strength;
f_l = expected confining stress in concrete core;
$f_{u,l}$ = tensile strength of longitudinal reinforcement;
$f_{u,t}$ = tensile strength of transverse reinforcement;
$f_{y,l}$ = yield strength of longitudinal reinforcement;
$f_{y,t}$ = yield strength of transverse reinforcement;
H_w = specimen height;
L_w = cross-sectional length;
P_c = contribution of concrete to load response;
s = transverse reinforcement spacing;
t_w = cross-sectional thickness
ε_{t0} = maximum tensile strain prior to monotonic or cyclic loading;
$\bar{\varepsilon}_{measured}$ = measured deformation capacity;
$\bar{\varepsilon}_{predicted}$ = predicted deformation capacity;
ρ_s = volumetric reinforcement ratio;
$\rho_{l,be}$ = longitudinal reinforcement ratio;
ρ_x = transverse reinforcement ratio parallel to the long dimension of the cross section; and
ρ_y = transverse reinforcement ratio parallel to the short dimension of the cross section.

References

Acevedo, C. (2010). "Seismic vulnerability of non-special boundary elements of shear walls under axial force reversals." Florida International Univ., Miami.

ACI (American Concrete Institute). (1995). "Building code requirements for reinforced concrete." *ACI 318-95*, Farmington Hills, MI.

ACI (American Concrete Institute). (2005). "Building code requirements for reinforced concrete." *ACI 318-05*, Farmington Hills, MI.

ACI (American Concrete Institute). (2014). "Building code requirements for reinforced concrete." *ACI 318-14*, Farmington Hills, MI.

ASTM. (2014a). "Standard specification for deformed and plain carbon-steel bars for concrete reinforcement." *ASTM A615/A615M–14*, West Conshohocken, PA.

ASTM. (2014b). "Standard specification for deformed and plain low-alloy steel bars for concrete reinforcement." *ASTM A706/A706M–14*, West Conshohocken, PA.

Birely, A., Lehman, D., Lowes, L., Kuchma, D., Hart, C., and Marley, K. (2012). "Investigation of the seismic behavior and analysis of reinforced concrete structural walls." *Proc., 14th World Conf. on Earthquake Engineering*, International Association of Earthquake Engineering, Tokyo.

Chrysanidis, T. A., and Tegos, I. A. (2012). "The influence of tension strain of wall ends to their resistance against lateral instability for low-reinforced concrete walls." *Proc., 15th World Conf. on Earthquake Engineering*, International Association of Earthquake Engineering, Tokyo.

Creagh, A., et al. (2010). "Seismic performance of concrete special boundary elements." Univ. of Texas, Austin, TX.

EERI (Earthquake Engineering Research Institute). (2010). "The Mw 8.8 Chile earthquake of February 27, 2010." *EERI Special Earthquake Rep.*, Oakland, CA.

INN (Instituto Nacional de Normalización). (1996). "Earthquake resistant design of buildings." *NCh433.Of96*, Santiago, Chile (in Spanish).

INN (Instituto Nacional de Normalización). (2006). "Steel–hot rolled bars for reinforced concrete." *NCh204Of.2006*, Santiago, Chile (in Spanish).

INN (Instituto Nacional de Normalización). (2008). "Reinforced concrete—Design and calculation requirements." *NCh430.Of2008*, Santiago, Chile (in Spanish).

Mander, J. B., Priestley, M. J. N., and Park, R. (1988a). "Observed stress-strain behavior of confined concrete." *J. Struct. Eng.*, 10.1061/(ASCE)0733-9445(1988)114:8(1827), 1827–1849.

Mander, J. B., Priestley, M. J. N., and Park, R. (1988b). "Theoretical stress-strain model for confined concrete." *J. Struct. Eng.*, 10.1061/(ASCE)0733-9445(1988)114:8(1804), 1804–1826.

Massone, L. M. (2013). "Fundamental principles of the reinforced concrete design code changes in Chile following the Mw 8.8 earthquake in 2010." *Eng. Struct.*, 56, 1335–1345.

Massone, L. M., Bonelli, P., Lagos, R., Luders, C., Moehle, J., and Wallace, J. W. (2012). "Seismic design and construction practices for RC structural wall buildings." *EERI Earthquake Spectra*, 28(S1), S245–S256.

MINVU (Ministerio de Vivienda y Urbanismo). (2010). "Regulation fixing the requirements for design and calculation of concrete and repeal of decree N°117, of 2010." *D.S. N°60*, Santiago, Chile (in Spanish).

Moehle, J. P., Ghodsi, T., Hooper, J. D., Fields, D. C., and Gedhada, R. (2011). "Seismic design of cast-in-plane concrete special structural walls and coupling beams." *GCR 11-917-11REV1*, NIST, Gaithersburg, MD.

Paulay, T., and Priestley, M. J. N. (1993). "Stability of ductile structural walls." *ACI Struct. J.*, 90(4), 385–392.

Richart, F. E., Brandtzaeg, A., and Brown, R. L. (1929). "The failure of plain and spirally reinforced concrete in compression." Univ. of Illinois, Urbana, IL.

Scott, B. D., Park, R., and Priestley, M. J. N. (1982). "Stress-strain behavior of concrete confined by overlapping hoops at low and high strain rates." *ACI J.*, 79(2), 13–27.

Telleen, K., Maffei, J., Heintz, J., and Dragovich, J. (2012). "Practical lessons for concrete wall design, based on studies of the 2010 Chile earthquake." *Proc., 15th World Conf. on Earthquake Engineering*, International Association of Earthquake Engineering, Tokyo.

Thomsen, J. H., and Wallace, J. W. (1994). "Lateral load behavior of reinforced concrete columns constructed using high strength materials." *ACI Struct. J.*, 91(5), 605–615.

Wallace, J. W., et al. (2012). "Damage and implications for seismic design of RC structural wall buildings." *EERI Earthquake Spectra*, 28(S1), S281–S299.

Welt, T. S. (2015). "Detailing for compression in reinforced concrete wall boundary elements: Experiments, simulations, and design recommendations." Ph.D. thesis, Univ. of Illinois, Urbana-Champaign, IL.